Journal of Inflammation Research

Dovepress
Taylor & Francis Group

Open Access Full Text Article

ORIGINAL RESEARCH

TLR4 Induces PANoptosis in Annulus Fibrosus Cells by Activating NLRP12 in Intervertebral Disc Degeneration

Feng Zheng[1,*], Linhai Cao[2,*], Jiawei Fu[2,*], Menglin Luo[3], Wenbo Yue[1], Yulin Ma[1], Binghan Chen[4], Yu Zhai[2], Chenhao Liu[1,2]

[1]Department of Orthopedics, Qinghai Provincial People's Hospital, Xining, Qinghai, People's Republic of China; [2]Department of Orthopedics, The Second Affiliated Hospital of Army Medical University, Chongqing, People's Republic of China; [3]Department of Laboratory, Chongqing Xiqu Hospital, Chongqing, People's Republic of China; [4]Department of Gastroenterology, People's Hospital of Anguo, Baoding, Hebei, People's Republic of China

*These authors contributed equally to this work

Correspondence: Chenhao Liu, Department of Orthopedics, Qinghai Provincial People's Hospital, Xining, Qinghai, 810007, People's Republic of China, Email juggmore@163.com; Yu Zhai, Department of Orthopedics, The Second Affiliated Hospital of Army Medical University, Chongqing, 400038, People's Republic of China, Email zhaiyu9501@tmmu.edu.cn

Purpose: Intervertebral disc degeneration (IVDD), a common degenerative disorder, is characterized by chronic inflammation and progressive cell death. PANoptosis, an integrated form of programmed cell death that merges pyroptosis, apoptosis, and necroptosis, has recently emerged as a key contributor to degenerative diseases. Although Toll-like receptor 4 (TLR4) and NLRP12 are known to regulate inflammatory signaling and cell death, their roles in mediating annulus fibrosus cells (AFCs). This study investigated how the TLR4–NLRP12 axis regulates AFC PANoptosis and contributes to IVDD progression.

Methods: Single-cell RNA sequencing (scRNA-seq) profiled cell heterogeneity and PANoptosis-related signaling in healthy/degenerative annulus fibrosus (AF) tissues. An in vitro IVDD model was established by treating AFCs with TNF-α to mimic inflammation. NLRP12 knockdown was performed via lentiviral transduction. PANoptosis was assessed by Western blot (cleaved-Caspase-1, cleaved-Caspase-3, p-MLKL, c-GSDMD), TUNEL staining, and flow cytometry. In vivo, a rat IVDD model was induced by acupuncture puncture, followed by TLR4 knockdown via lentiviral injection. X-ray imaging was used to assess intervertebral space height, histology to evaluate disc morphology, and TUNEL assay to detect annulus fibrosus cell death.

Results: scRNA-seq revealed an increased abundance of Fibro-AFCs and Adh-AFCs in IVDD, alongside enrichment of cell death-related pathways. PANoptosis-related gene expression and cell death scores were elevated in degenerative samples. In vitro, TLR4 activation induced PANoptosis in AFCs, which was attenuated by either TLR4 inhibition or NLRP12 knockdown. Formation of the PANoptosome complex-characterized by colocalization of Caspase-8, ASC, and RIPK3-was observed in degenerative AFCs. In vivo, TLR4 silencing ameliorated IVDD pathology, as evidenced by improved disc height, and reduced cell death. To our knowledge, this is the first study to identify the occurrence of PANoptosis in AFCs.

Conclusion: TLR4 promotes PANoptosis in AFCs through NLRP12 activation, driving IVDD pathogenesis. The TLR4-NLRP12-PANoptosis presents a potential therapeutic target for IVDD.

Keywords: TLR4, NLRP12, PANoptosis, annulus fibrosus cells, intervertebral disc degeneration, inflammatory microenvironment, single-cell RNA sequencing

Introduction

Low back pain is a leading cause of global disability, and intervertebral disc degeneration (IVDD) is one of its most common pathological underpinnings.[1] IVDD is a progressive pathological process characterized by structural disruption and cellular dysfunction within the disc, ultimately leading to biomechanical instability and chronic inflammation.[2] Among the major components of the intervertebral disc, the annulus fibrosus (AF) plays a crucial role in maintaining disc

Received: 29 July 2025
Accepted: 23 November 2025
Published: 1 December 2025

integrity by providing tensile strength and enclosing the nucleus pulposus.[3] During IVDD, annulus fibrosus cells (AFCs) undergo profound pathological alterations, including extracellular matrix (ECM) degradation, increased fibrosis, phenotypic transition, and inflammatory activation.[4] These changes compromise the structural and mechanical properties of the disc, accelerate tissue breakdown, and contribute to the chronic degenerative cascade. Despite the central role of AFCs in IVDD pathogenesis, the underlying regulatory mechanisms driving their degeneration remain incompletely understood.

PANoptosis is a recently identified form of programmed cell death that simultaneously engages pyroptosis, apoptosis, and necroptosis through the assembly of the PANoptosome complex.[5] PANoptosis is a unique, inflammatory programmed cell death pathway characterized by the concomitant activation of pyroptosis, apoptosis, and necroptosis, which cannot be fully accounted for by any of these pathways alone. Its execution is regulated by the assembly of a multifaceted protein complex termed the PANoptosome, which recruits key molecules such as ASC, RIPK3, and Caspase-8, among others. This complex serves as a molecular platform for the simultaneous activation of the three death pathways. In recent years, PANoptosis has gained increasing attention in IVDD research, as excessive cell death and inflammation are pivotal drivers of disease progression. For instance, one study demonstrated that PANoptosis occurs in nucleus pulposus cells (NPCs) and that L-BAIBA inhibits this process while promoting ECM synthesis via the AMPK/NF-κB pathway; similarly, another study showed that Kongensin A suppresses PANoptosis in NPCs by upregulating TAK1 and alleviates IVDD progression.[6] With attention growing on PANoptosis in IVDD, current research has predominantly focused on NPCs, leaving the relationship between PANoptosis and AFCs unexplored. Our previous research demonstrated that AFCs undergo apoptosis during disc degeneration, consistent with findings reported by Jacobsen et al[7,8] Additionally, studies by Yao et al[9] have shown that AFCs experience pyroptosis in the degenerative process. Drawing from these studies, we hypothesize that PANoptosis is likely involved in the degeneration of AFCs. However, PANoptosis has not been directly demonstrated in AFCs.

Toll-like receptor 4 (TLR4), as a key molecule connecting inflammation and cell death, has been confirmed to be involved in the pathological process of various degenerative diseases by activating downstream signaling pathways.[10] Additionally, NLRP12, as a negative regulatory factor of the NLR family, plays an important role in the balance between inflammatory signal transduction and cell death.[11] A study found that Heme + PAMPs induce the expression of NLRP12 through the TLR2/4-IRF1-ROS axis. NLRP12 assembles the PANoptosome to activate caspase-8/RIPK3 and cleaved-Caspase-1, mediates PANoptosis and the release of inflammatory factors, and aggravates hemolysis-related tissue damage.[5] However, in the inflammatory microenvironment of IVDD, it remains unclear whether NLRP12 serves as a key connector molecule between TLR4 and PANoptosis. While existing studies have demonstrated that TLR4 can exacerbate IVDD through inflammatory signaling, research on the impact of NLRP12 on IVDD remains notably scarce.

Based on this background, this study aims to explore for the first time the regulatory role of the TLR4 signaling pathway in PANoptosis of AFCs and clarify the mediating mechanism of NLRP12 as a key molecule. The research results will provide a new perspective for analyzing the pathogenesis of IVDD and lay a theoretical foundation for the development of intervention strategies targeting cell death pathways.

Materials and Methods

Single-Cell RNA Sequencing (scRNA-Seq) Analysis

We analyzed the publicly available single-cell RNA sequencing dataset GSE230809, which included 46,961 cells from three healthy AF samples and ten IVDD cases. Quality control was performed by filtering cells with feature counts between 300 and 8000, total RNA counts ranging from 500 to 60,000, and excluding cells with mitochondrial gene expression exceeding 20% or hemoglobin genes surpassing 10%. The data were normalized and subjected to principal component analysis (PCA) for dimensionality reduction, followed by UMAP clustering at a resolution of 0.5 to identify distinct cell populations. Cell type annotation was performed by integrating UMAP projections, hierarchical clustering, and known marker genes from existing literature. Differential gene expression analysis between healthy and IVDD groups was conducted using Seurat's FindMarkers function. Functional enrichment analysis, including Gene Ontology (GO) and KEGG pathway analysis, was performed to elucidate biological differences, supplemented by gene set enrichment analysis (GSEA) for pathway-level comparisons. Pseudotime trajectory analysis was carried out using Monocle 2 (v2.10.1) to explore dynamic transcriptional changes across

cell states. Additionally, gene set variation analysis (GSVA) was applied to evaluate pathway activity within clusters using the MSigDB c5.go.v2023.2.Hs.symbols.gmt gene set. To investigate intercellular signaling, we employed CellChat to infer ligand-receptor interactions and communication networks, focusing on pathways that exhibited significant differences between healthy and degenerated discs.

RNA Sequencing Analysis

RNA sequencing (RNA-seq) was conducted by Wuhan Metaware Biotechnology Company (Wuhan, China). Total RNA was extracted on ice using TRIzol reagent (Thermo Fisher Scientific, MA, USA). RNA concentration and purity were measured with a NanoDrop 2000 spectrophotometer (Thermo Fisher Scientific), while RNA integrity was assessed using the RNA Nano 6000 Assay Kit on the Agilent Bioanalyzer 2100 system (Agilent Technologies, CA, USA). Subsequently, the cDNA library was quality-checked using the same Agilent Bioanalyzer 2100 system. RNA-seq was performed on the Illumina NovaSeq platform. Raw sequencing data were processed to generate clean reads by removing adapter-containing reads, poly-N sequences, and low-quality reads. Clean reads were mapped to the reference *Rattus norvegicus* genome using HISAT2, followed by transcript reconstruction with StringTie. Gene expression levels were quantified as fragments per kilobase of transcript per million mapped fragments (FPKM). Differential gene expression analysis was performed using the DESeq R package (version 1.10.1). Genes were considered significantly differentially expressed if they met the thresholds of a false discovery rate (FDR) < 0.05 and $|\log2 \text{ fold change}| \geq 1$. Finally, KOBAS software was used to perform statistical enrichment analyses of differentially expressed genes in GO terms, KEGG pathways, and GSEA.

Isolation and Culture of AFCs

Under sterile conditions, AF tissue was isolated and cut into approximately 1 mm^3 fragments using ophthalmic scissors. For each isolation, AF tissues from 8 rats were pooled and digested with 0.4% type II collagenase and 0.01% type V hyaluronidase at 37 °C for 90 min. Tissue debris was removed using a 70-μm cell strainer, and the remaining suspension was centrifuged at 400 × g for 5 min. The supernatant was discarded, and the pellet was resuspended in complete medium consisting of Dulbecco's modified Eagle medium/F-12 (Viva Cell, Shanghai, China), 10% fetal bovine serum (Gibco, NY, USA), and 1% penicillin/streptomycin (Beyotime, Shanghai, China). Cells were cultured at 37 °C in a cell incubator with 5% CO_2. The medium was replaced every 3 days, and AFCs were passaged when confluency reached 80–90%. The third generation of AFCs was used for subsequent analysis. For the in vitro IVDD model, AFCs were treated with 20 ng/mL of TNF-α (MCE, NJ, USA) for 24 hours to mimic the inflammatory microenvironment.

Western Blot Analysis

AFCs were lysed using RIPA lysis buffer (Beyotime), and protein concentrations were determined with a BCA assay kit (Solarbio, Beijing, China). Lysates were mixed with 1/5 volume of loading buffer, followed by incubation in boiling water for 10 min. Proteins were separated using sodium dodecyl sulfate-polyacrylamide gel electrophoresis (SDS-PAGE) and subsequently transferred to PVDF membranes. These membranes were blocked with 5% skim milk for 1 h before being incubated with primary antibodies at 4°C overnight. The primary antibodies included cleaved-Caspase 1 (1:2000, Invitrogen, CA, USA, PA5-99390), cleaved-Caspase 3 (1:1000, Proteintech, IL, USA, 25128-1-AP), MLKL (1:5000, Proteintech, 66675-1-Ig), p-MLKL (1:1000, Invitrogen, MA5-32752), c-GSDMD (1:2000, abcam, UK, ab215203), and GAPDH (1:10000, Proteintech, 60004-1-Ig). After washing with TBST, the PVDF membranes were incubated with secondary antibodies for 1 h. The secondary antibodies employed were Goat Anti-Mouse IgG (H + L) HRP (1:20000, Absin, Shanghai, China) or Goat Anti-Rabbit IgG (H + L) HRP (1:20000, Absin). Target protein expression was detected using Clarity Western ECL Substrate (Bio-Rad, CA, USA) and a ChemiDoc imaging system (Bio-Rad), and analyzed with ImageJ software. All results were quantified and normalized to GAPDH.

TUNEL Staining Assay

TUNEL staining was performed to assess apoptosis in cultured AFCs. Cells were seeded on sterile glass coverslips in 6-well plates and treated as indicated. After treatment, cells were fixed with 4% paraformaldehyde for 30 minutes at room temperature, followed by permeabilization with 0.1% Triton X-100 for 10 minutes. Apoptotic cells were detected using a

TUNEL apoptosis detection kit (Bio-Rad), following the manufacturer's instructions. Briefly, the labeling reaction was carried out in a humidified chamber at 37°C for 1 hour in the dark. After washing, nuclei were counterstained with DAPI for 5 minutes. Coverslips were mounted with antifade reagent and examined using a fluorescence microscope (Olympus, Tokyo, Japan). The apoptosis index was calculated as the percentage of TUNEL-positive cells relative to the total number of nuclei.

Apoptosis Detection by Flow Cytometry

Apoptosis in AFCs was quantified using flow cytometry with Annexin V-PE/7-AAD double staining. After treatment, cells were harvested by trypsinization without EDTA, washed twice with cold PBS, and resuspended in 1× binding buffer at a concentration of 1×10^6 cells/mL. A total of 100 μL of the cell suspension was incubated with 5 μL Annexin V-PE and 5 μL Phycoerythrin (PE) for 15 minutes at room temperature in the dark, according to the manufacturer's instructions of the Annexin V-PE/7-AAD Apoptosis Detection Kit (Roche, IN, USA). After staining, 400 μL of binding buffer was added, and samples were immediately analyzed using a flow cytometer. At least 10,000 events were recorded per sample. Early apoptotic cells (Annexin V^+/PE^-) and late apoptotic or necrotic cells (Annexin V^+/PE^+) were quantified, and the apoptosis rate was calculated as the sum of early and late apoptotic populations.

Immunofluorescence Staining

AFCs were seeded into confocal culture dishes and treated as indicated. After treatment, cells were fixed with 4% paraformaldehyde for 20 minutes at room temperature and permeabilized with 0.1% Triton X-100 for 10 minutes. Non-specific binding was blocked with 5% BSA for 1 hour. Cells were then incubated with primary antibodies against Caspase-8 (1:100, Invitrogen, MA1-41280), RIPK3 (1:200, Invitrogen, 703750), and ASC (1:200, Invitrogen, PA5-50915) overnight at 4°C. After washing, cells were incubated with appropriate fluorophore-conjugated secondary antibodies for 1 hour at room temperature in the dark. Nuclei were counterstained with DAPI. Coverslips were mounted with antifade reagent and imaged using a fluorescence microscope. Colocalization of proteins was evaluated to assess PANoptosome formation.

Establishment of the IVDD Rat Model

Under aseptic conditions, male Sprague-Dawley rats (8 weeks old) were anesthetized by intraperitoneal injection of sodium pentobarbital (40 mg/kg). The coccygeal intervertebral discs were located via palpation and confirmed by lateral X-ray. Under fluoroscopic guidance, a 20G needle was inserted perpendicularly into the AF of the target disc to a depth of 5 mm, then rotated 360° for 30 seconds. At 4 weeks post-puncture, the intervertebral disc tissues were harvested for histological sectioning, magnetic resonance imaging (MRI), and biochemical analysis. All animal experiments were approved by the Laboratory Animal Welfare and Ethics Committee of Qinghai Provincial People's Hospital. Twelve rats were randomly assigned to four experimental groups (n = 3 per group): Sham, IVDD, IVDD + LV-control, and IVDD + LV-shTLR4. For in vivo delivery, a total of 5 μL lentivirus (1×10^8 TU/mL) was slowly injected into the punctured disc using a microsyringe immediately after the acupuncture procedure.

Histological Staining

Rat intervertebral discs were harvested, fixed in 4% paraformaldehyde for 48 hours, decalcified in 10% EDTA for three weeks, and embedded in paraffin. Serial sagittal sections (5 μm thick) were prepared for histological and apoptosis analyses. H&E staining was performed following standard procedures: sections were deparaffinized, rehydrated, stained with hematoxylin for 5 minutes, rinsed, counterstained with eosin for 2 minutes, dehydrated, cleared, and mounted. For Safranin O/Fast Green (SO/FG) staining, sections were stained with Fast Green for 5 minutes, rinsed in acetic acid, then stained with Safranin O for 5 minutes, followed by dehydration and mounting.

TUNEL staining was performed on paraffin sections to detect apoptotic cells in the AF region. Sections were processed using a commercial TUNEL apoptosis detection kit (Beyotime), following the manufacturer's protocol. Briefly, sections were dewaxed, rehydrated, permeabilized with proteinase K, and incubated with TUNEL reaction mixture at 37°C for 1 hour in the dark. Nuclei were counterstained with DAPI, and apoptotic cells (TUNEL-positive)

were visualized using a fluorescence microscope. Quantification was performed from three randomly selected fields per section.

X-Ray Analysis

Lateral X-ray imaging of rat tails was performed to evaluate intervertebral disc height after AF puncture and treatment. The scanning parameters were set as follows: 63 mA exposure and 35 kV penetration. Intervertebral disc height index (DHI) was calculated using ImageJ software, with changes in DHI expressed as DHI% (postoperative DHI/preoperative DHI × 100%).

Lentiviral Construction and Transduction

All lentiviral vectors, including shRNA constructs targeting TLR4 and NLRP12, as well as control vectors, were designed and synthesized by GeneChem (Shanghai, China). The target sequences for rat TLR4 and NLRP12 shRNA were as follows: shTLR4: 5'-GACCAGAAATTGCTGAGTT-3'; shNLRP12: 5'-GCAGATGAACTGGTATTAT-3'. AFCs were seeded in six-well plates and transduced with lentivirus at a multiplicity of infection (MOI) of 20 in the presence of polybrene (5 μg/mL). After 24 hours of incubation, the medium was replaced with fresh complete medium, and cells were cultured for an additional 48–72 hours prior to downstream analysis. Knockdown efficiency was confirmed by qPCR and Western blot. For in vivo delivery, lentivirus was injected directly into the AF region of rat tail discs using a microsyringe immediately after needle puncture.

Data Analysis

All experiments were performed in three biological replicates with technical triplicates. Statistical analysis was performed using GraphPad Prism 11 (Graphpad Software Inc., MA, USA). Data are expressed as mean ± SD. Two-group comparisons were analyzed using an unpaired *t*-test. Multiple comparisons used one-way ANOVA followed by Bonferroni's post hoc test. $p < 0.05$ was considered statistically significant.

Results

scRNA-Seq Analysis Reveals Cellular Remodeling and Subtype Shifts in Degenerative AF Tissue

We analyzed the publicly available single-cell RNA-sequencing dataset GSE230809, which includes three samples of healthy AF tissue and ten samples from IVDD cases. To eliminate low-quality cells and minimize RNA contamination, we performed preprocessing and quality control on the dataset, retaining a total of 43,421 cells for downstream analysis.

Using the Seurat standard pipeline and unsupervised Uniform Manifold Approximation and Projection (UMAP) clustering, we identified distinct cell populations. Cluster annotation was based on UMAP projection, hierarchical clustering, and expression patterns of canonical markers reported in the literature (Figure 1A and C). The following AF cell subtypes were identified:

- Fibrotic-like AF cells (Fibro-AFCs): characterized by expression of COL1A1 and FBLN[12]
- Chondrocyte-like AF cells (Chon-AFCs): expressing SOX9 and ACAN[13]
- Homeostatic AF cells (Homeo-AFCs): marked by RSP29 and CCN3[14]
- Adhesive AF cells (Adh-AFCs): expressing MSMO1 and HMGCS1[15]
- Regulatory AF cells (Reg-AFCs): marked by CHI3L1 and CXCL2[16]

The relative proportions of each subpopulation are shown in Figure 1B, with Homeo-AFCs being the most abundant and Reg-AFCs the least represented. Figure 1C and H shows the marker genes for each cell cluster. Next, we compared the distribution and relative proportions of AF subtypes between healthy and degenerative samples (Figure 1D and E). Notably, Fibro-AFCs and Adh-AFCs were significantly increased in IVDD samples, while Chon-AFCs and Homeo-AFCs were markedly decreased. Reg-AFCs showed a slight reduction.

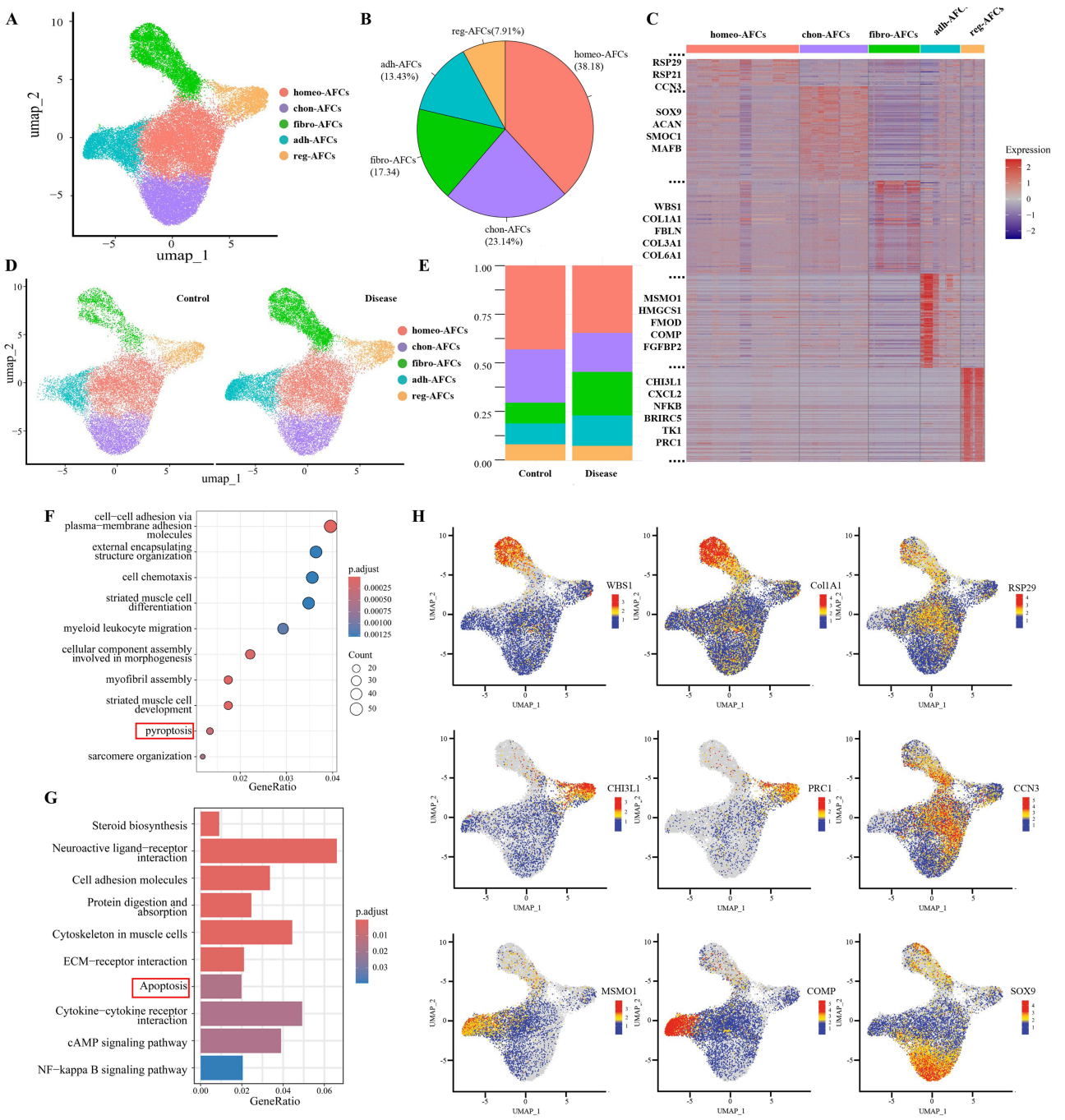

Figure 1 Single-cell RNA sequencing reveals cellular heterogeneity and functional pathways in intervertebral disc tissues. (**A**) UMAP visualization of 43,421 cells from the human NP tissue, dyed according to cell types. (**B**) Pie chart of the cell type ratio in intervertebral disc tissues. (**C**) Heatmap of differentially expressed genes among different AFCs subpopulations, including homo-AFCs, chon-AFCs, fibro-AFCs, and pro-AFCs. (**D** and **E**) Comparison of cell type distributions between control and disease groups. (**F**) GO enrichment analysis for differentially expressed genes between control and disease groups. Enriched pathways related to cell death and inflammation are highlighted with red box. (**G**) KEGG enrichment analysis highlight the top enriched pathways. Enriched pathways related to cell death and inflammation are highlighted with red box. (**H**) Expression distribution of representative marker genes across different cell clusters.

We subsequently performed Gene Ontology (GO) and Kyoto Encyclopedia of Genes and Genomes (KEGG) pathway enrichment analyses for the healthy and IVDD groups (Figure 1F and G). GO terms enriched in the degenerative group included cell-cell adhesion via plasma membrane adhesion molecules, cell chemotaxis, myofibril assembly, cellular component assembly involved in morphogenesis, and pyroptosis. KEGG analysis revealed enrichment in cell adhesion molecules, ECM-receptor interaction, apoptosis, cAMP signaling, and NF-κB signaling pathway.

Interestingly, both GO and KEGG analyses revealed enrichment of pathways related to cell death, prompting us to hypothesize that PANoptosis, a form of programmed cell death integrating pyroptosis, apoptosis, and necroptosis, might be occurring in IVDD.

PANoptosis Activation Detected in AFCs During IVDD

PANoptosis is an inflammatory form of programmed cell death (PCD) regulated by the formation of the PANoptosome complex and triggered by specific signals. It integrates key molecular features of pyroptosis, apoptosis, and necroptosis.

To investigate whether PANoptosis occurs in IVDD, we conducted Gene Set Enrichment Analysis (GSEA) on several relevant pathways, including the NLRP1 inflammasome complex, NLRP3 inflammasome complex, apoptosis, necroptosis, and pyroptosis (Figure 2A). GSEA results revealed that PANoptosis-related gene sets were significantly downregulated in healthy samples relative to degenerative samples, indicating their upregulation in the latter. We next calculated pyroptosis, apoptosis, and necroptosis scores for each sample. All three scores were significantly elevated in the IVDD group compared to controls (Figure 2B), supporting the activation of PANoptotic signaling during disc degeneration.

To further explore the cellular progression dynamics, we performed pseudotime trajectory analysis. Adh-AFCs were positioned at the early stage of the pseudotime axis, Fibro-AFCs were primarily located at the terminal end, distributed in

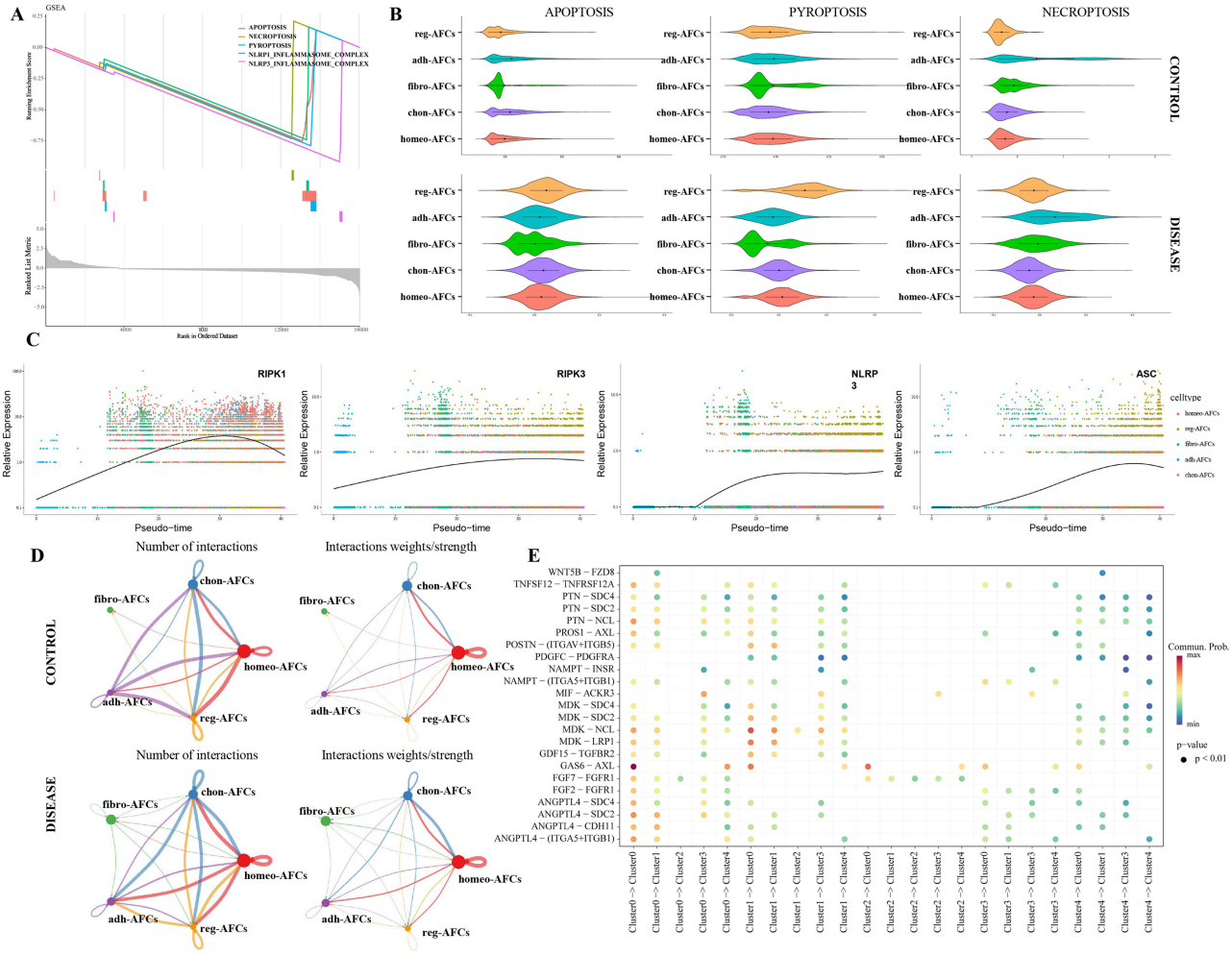

Figure 2 Single-cell trajectory analysis and interaction network reveal molecular mechanisms in AFCs. (**A**) GSEA analysis of PANoptosis-related pathways. (**B**) Apoptosis, pyroptosis, and necroptosis scores across distinct cell subpopulations. (**C**) Pseudotime trajectory analysis of key genes (RIPK1, RIPK3, NLRP3, ASC) involved in PANoptosis. (**D**) Interaction network constructed by CellPhoneDB showing potential interactions between different cell clusters. (**E**) Cell interaction network analysis based on ligand-receptor pairs.

https://doi.org/10.2147/JIR.S556950

the late stage of the trajectory, while Homeo-AFCs were evenly distributed across all pseudotime stages (Figure S1A). This suggests a potential differentiation trajectory from adhesive to fibrotic phenotypes during disease progression. To further examine the association between degeneration and PANoptosis, we analyzed the expression of PANoptosis-related genes along the pseudotime axis. Key genes such as RIPK1, RIPK3, NLRP3, and ASC were found to be markedly upregulated in late-stage AFCs (Figure 2C), implicating enhanced PANoptotic activity in these cells. Finally, we evaluated intercellular communication patterns within AF subpopulations. The IVDD group exhibited significantly increased frequency and strength of cell-cell interactions compared to the healthy group (Figure 2D and E), indicating a more active and inflammatory intercellular environment that may promote PANoptosis.

Collectively, these findings suggest that PANoptosis is likely activated in degenerative AF tissues and that late-stage AFCs may serve as a central hub for this process.

TLR4 Drives PANoptosis in AFCs

To further verify the occurrence of PANoptosis in degenerative AFCs, we treated AFCs with tumour necrosis factor-alpha (TNF-α) to simulate the degenerative inflammatory environment. Western blot analysis showed increased expression of PANoptosis-related proteins, including cleaved-Caspase-1, cleaved-Caspase-3, MLKL, phosphorylated MLKL (p-MLKL), and cleaved Gasdermin D (c-GSDMD), in TNF-α-treated cells compared to the control and DMSO groups (Figure 3A and B). This indicates that inflammation-induced degeneration of AFCs leads to activation of PANoptosis. Immunofluorescence staining revealed the formation of PANoptosome complexes, marked by colocalization of Caspase-8, RIPK3, and ASC in TNF-α-treated cells (Figure 3C). These aggregates (white arrows) provide morphological evidence of PANoptosome assembly in degenerative AFCs.

To further investigate the molecular changes in degenerative AFCs, we performed transcriptome sequencing on TNF-α-treated and control groups. Heatmap and volcano plot exhibited the differentially expressed genes (Figure 3D and E), KEGG pathway enrichment analysis revealed significant involvement of the apoptosis pathway, while GO analysis showed enrichment in the NLRP1 inflammasome complex (Figure 3F), suggesting that TNF-α treatment triggers PANoptosis-related processes in AFCs. In addition, KEGG analysis also indicated activation of the Toll-like receptor signaling pathway, and Reactome analysis highlighted enrichment in the activated TLR4 signaling cascade. These findings imply a potential link between TLR4 activation and PANoptosis induction. To validate these results, GSEA was conducted on representative pathways, including apoptosis, Toll-like receptor signaling, and activated TLR4 signaling. The results were consistent with the enrichment analyses described above (Figure 3G), further supporting the role of TLR4 activation in promoting PANoptosis in this inflammatory model.

TLR4 Induces PANoptosis via NLRP12 Activation in AFCs

RKH acetate is a specific TLR4 inhibitor that directly binds TLR4 and blocks its downstream signaling.[17] To explore the role of TLR4 in AFC PANoptosis, AFCs were treated with RKH acetate. WB showed that RKH acetate reversed the TNF-α-induced upregulation of cleaved-Caspase-1, cleaved-Caspase-3, MLKL, p-MLKL, and c-GSDMD (Figure 4A and B), indicating that inhibition of TLR4 alleviates PANoptosis in AFCs. TUNEL staining revealed an increase in apoptotic cells in the TNF-α group, which was reduced after TLR4 inhibition (Figure 4C and D). FC further confirmed that TLR4 blockade attenuated TNF-α-induced apoptosis (Figure 4E and F).

To further validate the involvement of TLR4, AFCs were infected with TLR4 knockdown (KD) lentivirus. WB showed that PANoptosis-related protein levels were significantly reduced in the KD group compared to the LV-ctrl group (Figure 4G and H). Consistently, TUNEL and FC analysis demonstrated decreased apoptosis following TLR4 silencing (Figure 4I–L). These findings suggest that TLR4 promotes PANoptosis in AFCs.

Among known PANoptosome inducers, ZBP1-, AIM2-, and NLRP12-mediated complexes have been identified.[18] ZBP1 and AIM2 are typically activated by viral stimuli, which are absent in the intervertebral disc environment.[19,20] Previous work by Sundaram et al demonstrated that TLR4 functions upstream of NLRP12 to promote PANoptosome assembly.[5] Based on this, we hypothesized that TLR4 may induce PANoptosis in degenerative AFCs via NLRP12. This hypothesis was supported by our transcriptomic heatmap, which showed increased expression of NLRP12-related genes in degenerative AFCs (Figure S1B). To verify the role of NLRP12, AFCs were treated with TLR4 agonist-1 (TEA), a

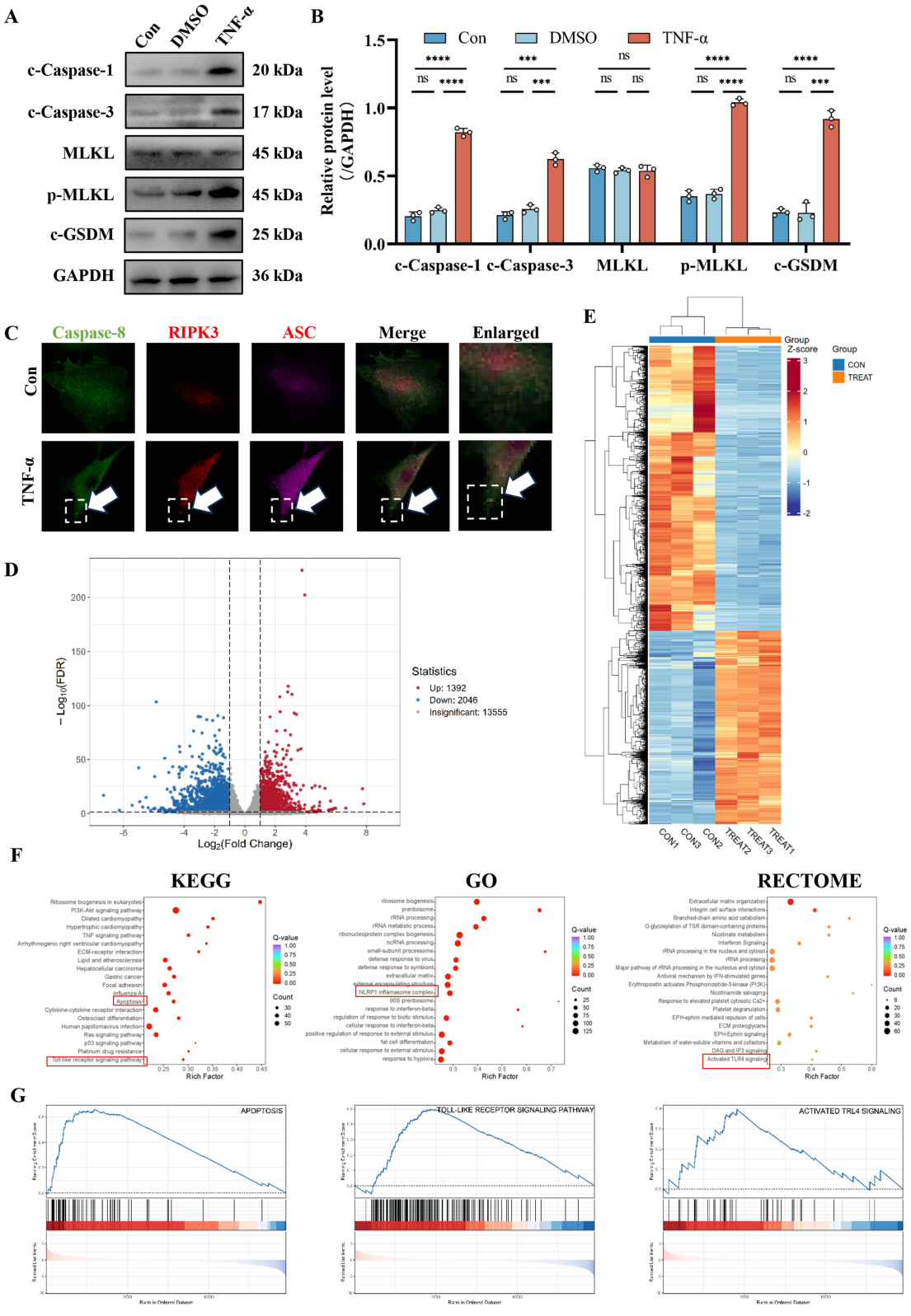

Figure 3 TLR4 Drives PANoptosis in Annulus Fibrosus Cells. (**A**) Western blot analysis of PANoptosis-related proteins (Caspase-1, Caspase-3, MLKL, p-MLKL, C-GSDMD) in Group Con, DMSO, and TNF-α. GAPDH serves as a loading control. (**B**) Quantification of relative protein levels in (**A**) normalized to GAPDH. (**C**) Immunofluorescence staining of Caspase-8, RIPK3, and ASC in Con group and TNF-α group. White arrows indicate the aggregated PANoptosome complex. (**D**) Heatmap of differentially expressed genes in AFCs between Con group and TNF-α group. (**E**) Volcano map of differentially expressed genes between Con and TNF-α groups. (**F**) GO analysis, KEGG analysis, and Reactome analysis of differentially expressed genes. Enriched pathways related to cell death and inflammation are highlighted with red box. (**G**) GSEA analysis of representative pathways (Apoptosis, Toll-like receptor signaling pathway, Activated tlr4 signaling) in AFCs. ***$p < 0.001$; ****$p < 0.0001$; ns indicates not significant.

https://doi.org/10.2147/JIR.S556950

potent TLR4 activator, with or without NLRP12 KD. WB showed that TEA significantly upregulated PANoptosis-related proteins, consistent with our earlier findings (Figure 4M and N). Notably, NLRP12 KD markedly suppressed the TEA-induced expression of these proteins compared to the TEA and TEA+LV-ctrl groups, indicating that TLR4 promotes PANoptosis through NLRP12 in AFCs. Consistent with the WB findings, TUNEL and FC analyses showed similar trends (Figure 4O–R). These findings confirm that TLR4 induces PANoptosis in AFCs through activation of NLRP12.

Inhibition of TLR4 Ameliorates IVDD in Rat Model

To evaluate the role of TLR4 in AF degeneration in vivo, lentiviral-mediated TLR4 knockdown was performed in rat AF tissue. X-ray imaging showed that TLR4 KD significantly alleviated disc height loss induced by acupuncture compared to the LV-ctrl group (Figure 5A and E).

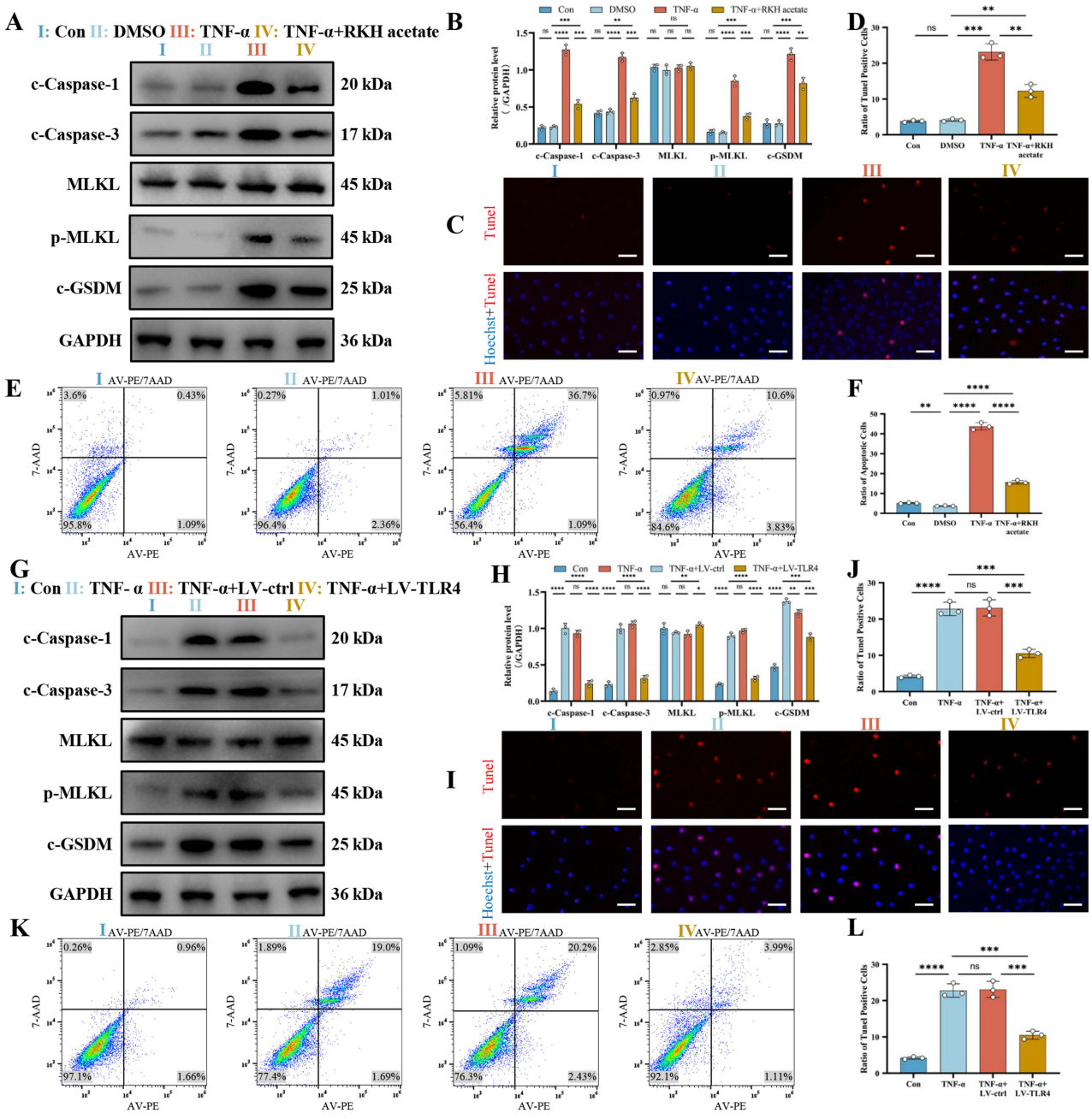

Figure 4 Continued.

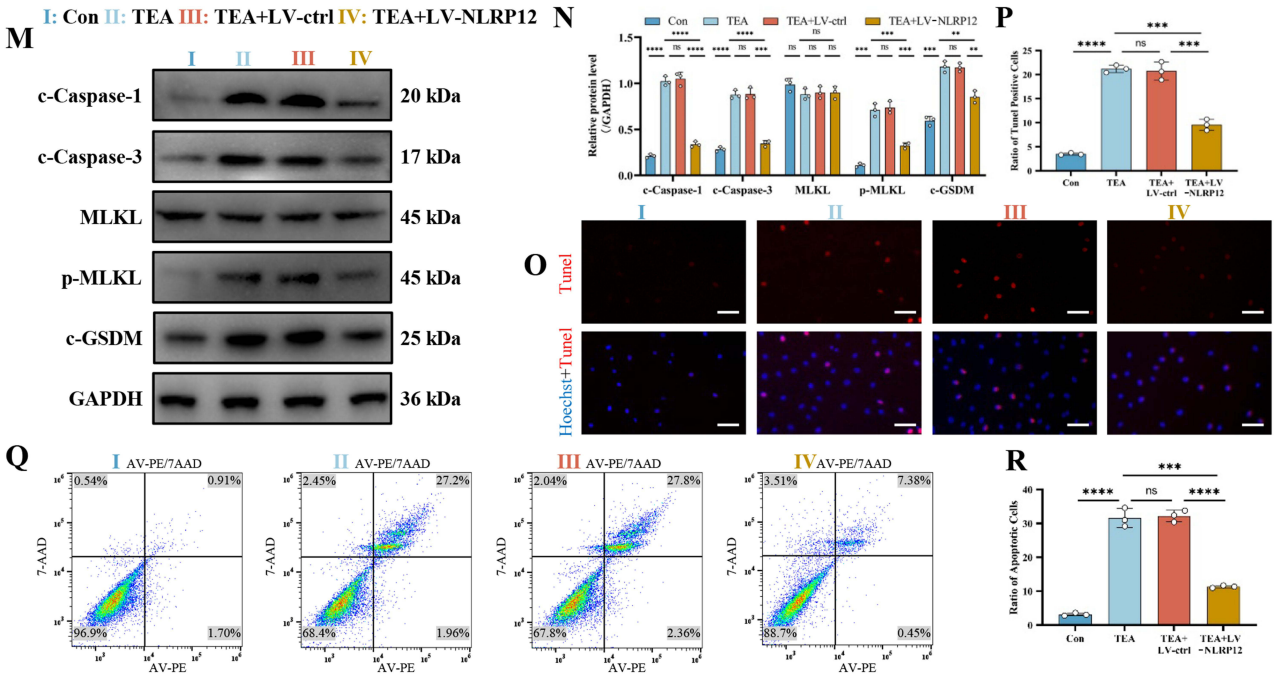

Figure 4 TLR4 Induces PANoptosis via NLRP12 Activation in AFCs. (**A** and **B**) Western blot analysis and quantification of PANoptosis-related proteins (Caspase-1, Caspase-3, MLKL, p-MLKL, C-GSDMD) in AFCs treated with Con, DMSO, TNF-α and TNF-α+RKH acetate. (**C**) TUNEL staining detecting AFCs apoptosis in Con, DMSO, TNF-α, and TNF-α+ RKH acetate groups. Apoptotic cells appear red, and nuclei are counterstained with Hoechst (blue). Scale bar = 40 μm. (**D**) Statistical analysis of TUNEL-positive apoptotic AFCs in (**C**). (**E**) Representative flow cytometry scatter plots detecting AFCs apoptosis in TNF-α, and TNF-α+ RKH acetate groups. (**F**) Statistical analysis of apoptotic AFCs in (**E**) determined by flow cytometry (n=3). (**G** and **H**) Western blot analysis and quantification of PANoptosis-related proteins in AFCs treated with Con, TNF-α, TNF-α+Lv-ctrl, and TNF-α+Lv-TLR4. (**I**) TUNEL staining detecting AFCs apoptosis in Con, TNF-α, TNF-α+Lv-ctrl, and TNF-α+Lv-TLR4 groups. Scale bar = 40 μm. (**J**) Statistical analysis of TUNEL-positive apoptotic AFCs in (**I**). (**K**) Representative flow cytometry scatter plots detecting AFCs apoptosis in Con, TNF-α, TNF-α +Lv-ctrl, and TNF-α+Lv-TLR4 groups. (**L**) Statistical analysis of apoptotic AFCs in (**K**) determined by flow cytometry (n=3). (**M** and **N**) Western blot analysis and quantification of PANoptosis-related proteins in AFCs treated with Con, TEA, TEA+Lv-ctrl, and TEA+Lv-NLRP12. (**O**) TUNEL staining detecting AFCs apoptosis in Con, TEA, TEA+Lv-ctrl, and TEA+Lv-NLRP12 groups. Scale bar = 40 μm. (**P**) Statistical analysis of TUNEL-positive apoptotic AFCs in (**O**). (**Q**) Representative flow cytometry scatter plots detecting AFCs apoptosis in Con, TEA, TEA+Lv-ctrl, and TEA+Lv-NLRP12 group. (**R**) Statistical analysis of apoptotic AFCs in (**Q**) determined by flow cytometry (n=3). **p < 0.01; ***p < 0.001; ****p < 0.0001; ns indicates not significant.

H&E staining revealed that TLR4 KD preserved the lamellar structure of the AF and reduced NP shrinkage, resulting in improved histological scores compared to the IVDD rats with LV-ctrl (Figure 5B and F). SO/FG staining indicated that GAG content, which was reduced in the IVDD group, was restored after TLR4 knockdown (Figure 5C). TUNEL staining showed increased apoptosis in IVDD discs, which was markedly reduced following TLR4 silencing (Figure 5D and G).

Collectively, these in vivo data demonstrate that suppressing TLR4 alleviates disc degeneration, further corroborating the critical role of TLR4 in regulating AF PANoptosis during IVDD. A schematic diagram of PANoptosis induced by TLR4-NLRP12 activation in degenerative AFCs is shown in Figure 6.

Discussion

In this study, we systematically explored the role of TLR4 signaling in AFCs during IVDD. scRNA-seq analysis revealed an increased proportion of fibroblast-like AFC subtypes and transcriptional enrichment of pyroptosis and apoptosis pathways in degenerative discs. Functional experiments showed that TNF-α stimulation induced activation of PANoptosis in AFCs, as evidenced by upregulation of cleaved-Caspase-1, cleaved-Caspase-3, MLKL, p-MLKL, and c-GSDMD, along with formation of PANoptosome structures. Transcriptomic analysis further identified TLR4 as a key upstream regulator, acting via NLRP12. In vivo, TLR4 knockdown mitigated disc degeneration and reduced PANoptosis in AFCs. Collectively, our findings indicate that PANoptosis occurs in degenerative AFCs, regulated by the TLR4-NLRP12 axis. To our knowledge, this is the first study to implicate PANoptosis as a relevant mode of cell death in AFCs during IVDD, providing novel insights into the degenerative process of the disc.

https://doi.org/10.2147/JIR.S556950

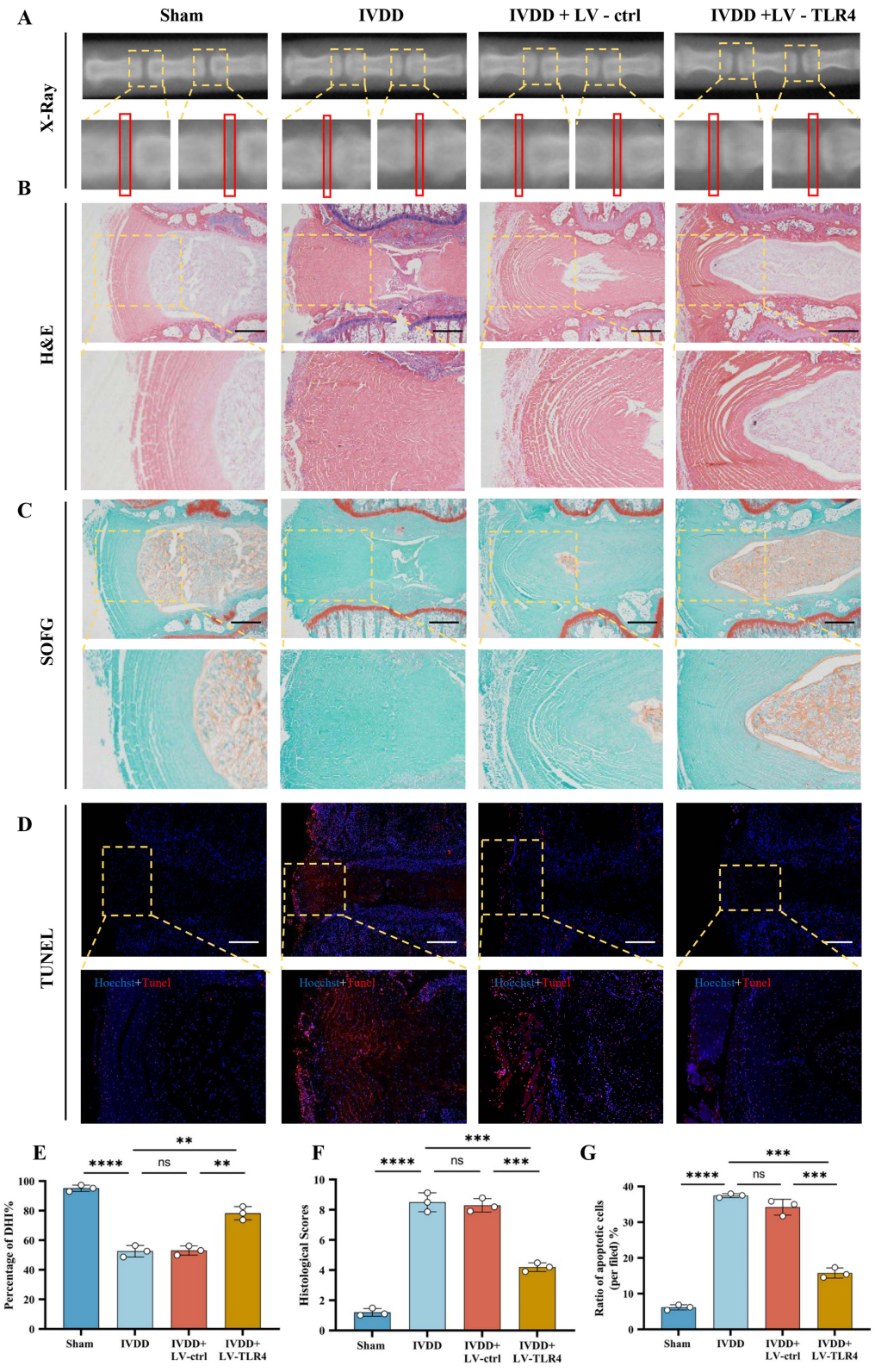

Figure 5 Inhibition of TLR4 Ameliorates IVDD in Rat Models. (**A**) X-ray images of intervertebral discs in rats subjected to different treatments. Disc heights are highlighted with red box. (**B**) H&E staining of intervertebral disc tissues from rats with various treatments. Scale bar = 500 μm. (**C**) SOFG staining of intervertebral disc tissues from rats with different treatments. Scale bar = 500 μm. (**D**) TUNEL staining of intervertebral disc tissues from rats under various treatments. Scale bar = 800 μm. (**E**) Quantitative analysis of DHI% (Disc Height Index percentage) based on X-ray results. (**F**) Histological score analysis of different treatments. (**G**) The ratio of apoptotic cells in AF tissue of rats shown by TUNEL staining. $^{**}p < 0.01$; $^{***}p < 0.001$; $^{****}p < 0.0001$; ns indicates not significant.

Recent studies have applied scRNA-seq to explore cellular heterogeneity in IVDD, with most focusing on NP samples.[21,22] These analyses have identified key immune, stromal, and degenerative cell populations involved in disc pathology. We reanalyzed the scRNA-seq dataset GSE230809, which included 3 healthy and 10 degenerative AF samples. After standard quality control and batch integration, 43,421 cells were retained for downstream analysis. Based on canonical markers reported in previous studies, we performed cell clustering and identified five distinct AFC subtypes: Fibro-AFCs, Chon-AFCs, Homeo-AFCs, Adh-AFCs, and Reg-AFCs. Among these, Fibro-AFCs were significantly enriched in IVDD samples and were closely associated with extracellular matrix remodeling and fibrosis. To further explore the biological changes in degenerative AF tissue, we performed GO and KEGG enrichment analyses using the ClusterProfiler package. GO terms enriched in the degenerative group included "cell-cell adhesion", "myofibril assembly", and "pyroptosis", while KEGG analysis highlighted pathways such as apoptosis, ECM-receptor interaction, and NF-κB signaling. Notably, both analyses revealed strong enrichment in cell death-related pathways, raising the possibility that PANoptosis may be involved in the degenerative process.

To evaluate the activation of programmed cell death pathways in degenerative AFCs, we calculated apoptosis, pyroptosis, and necroptosis scores using gene set-based module scoring. All three scores were significantly elevated in the degenerative group, suggesting simultaneous activation of multiple cell death programs. To further explore the temporal dynamics of these processes, we conducted pseudotime trajectory analysis using the Monocle3 package. This method, commonly used in scRNA-seq studies, enables inference of gene expression changes along a simulated degenerative trajectory. Our analysis revealed that Adh-AFCs were positioned at early pseudotime stages, while Fibro-AFCs were predominantly enriched at later stages, indicating that PANoptosis may occur in terminally activated AFC subsets. We next evaluated the expression patterns of RIPK1, RIPK3, NLRP3, and ASC-core components of the PANoptosome.[23] RIPK1 and RIPK3 are central to necroptotic signaling and can engage in PANoptotic complexes through interactions with Caspase-8.[24] NLRP3, a canonical inflammasome sensor, and ASC, an adaptor protein essential for inflammasome assembly, are also critical for PANoptosis execution.[25,26] Our pseudotime analysis revealed that these genes were significantly upregulated in late-stage AFCs, further supporting the involvement of PANoptosis in degenerative progression.

To mimic the inflammatory environment observed in degenerative AF tissue, we treated AFCs with TNF-α, a pro-inflammatory cytokine previously reported to participate in disc degeneration and immune-related matrix remodeling.[27,28] Upon stimulation, WB analysis revealed increased expression of cleaved-Caspase-1, cleaved-Caspase-3, p-MLKL, and c-GSDMD, which are canonical executioner molecules of pyroptosis, apoptosis, and necroptosis, respectively.[6,29] These results confirmed the activation of PANoptosis under degenerative-like stimulation. To further assess the assembly of PANoptosomes, IF staining was performed to detect Caspase-8, RIPK3, and ASC, which have been identified as core components of the PANoptosome complex in other inflammatory or infectious contexts.[6] Colocalization of these markers in TNF-α-treated AFCs supported the presence of functional PANoptosome aggregates, providing morphological evidence of PANoptosis. To gain insight into global transcriptomic changes induced by TNF-α, we conducted bulk RNA-seq analysis. AFCs were grouped into TNF-α-treated and control conditions. GO and KEGG enrichment analyses showed that TNF-α treatment upregulated genes involved in apoptosis, inflammasome activation, ECM-receptor interaction, and Toll-like receptor signaling, suggesting enhanced activation of inflammatory and cell death pathways. Reactome pathway analysis further highlighted enrichment in the activated TLR4 signaling cascade, implicating TLR4 as a key upstream modulator. To validate these findings, we performed GSEA on representative gene sets, including apoptosis, TLR signaling, and activated TLR4 signaling. These pathways were significantly enriched in the TNF-α-treated group, confirming that TLR4-driven signaling is a potential upstream regulator of PANoptosis in AFCs.

To confirm the upstream regulatory role of TLR4 in AFC PANoptosis, we first employed RKH acetate, a selective TLR4 inhibitor. WB, TUNEL, and flow cytometry results demonstrated that inhibition of TLR4 markedly reduced the expression of PANoptosis-related proteins and attenuated cell death in TNF-α-treated AFCs. To further validate these findings, we constructed a TLR4-knockdown lentiviral vector. Consistently, TLR4 silencing led to decreased levels of cleaved-Caspase-1, cleaved-Caspase-3, p-MLKL, and c-GSDMD, along with reduced TUNEL-positive and apoptotic cell populations. These results confirm that TLR4 contributes directly to PANoptosis induction in AFCs.

PANoptosis is executed via the formation of PANoptosomes-multiprotein complexes composed of key molecules such as ASC, RIPK3, and Caspase-8. Recent studies have defined three PANoptosome complexes with distinct sensors and

regulators: ZBP1-, AIM2-, and NLRP12-mediated complexes.[30] ZBP1- and AIM2-associated PANoptosis are generally activated in response to viral or microbial components, which are largely absent in the IVD microenvironment.[31] Based on this, we hypothesized that NLRP12 may be the dominant initiator of PANoptosome formation in AFCs. Transcriptomic analysis revealed that only NLRP12 was significantly upregulated in degenerative conditions, while ZBP1 and AIM2 showed no notable changes. To further evaluate the role of NLRP12, we performed rescue experiments using TEA, a potent TLR4 agonist. While TEA alone induced robust upregulation of PANoptosis-related proteins, co-treatment with NLRP12 knockdown markedly attenuated this response. Together, these data suggest that aberrant activation of the TLR4-NLRP12 axis may be a detrimental driver of AFC death and IVDD progression through PANoptosome assembly.

To validate TLR4 function in vivo, we knocked down TLR4 in a rat AF puncture model. TLR4 silencing alleviated disc height loss, preserved AF structure, and restored GAG content. TUNEL staining showed reduced apoptosis, indicating protective effects against cell death. These findings support that TLR4 contributes to IVDD progression by promoting AFC degeneration. Combined with our i*n vitro* data, we propose that aberrant TLR4 activation induces PANoptosis via NLRP12, exacerbating disc degeneration. This pathological mechanism is summarized in Figure 6.

Although TLR4 knockdown alleviated disc degeneration in vivo, the findings were primarily based on rodent models and in vitro assays. The needle puncture model utilized in this study, while effective, induces mechanical injury in nature. It should be noted that the invasive nature of this intervention can elicit inflammatory responses.[32] Human-derived AFCs

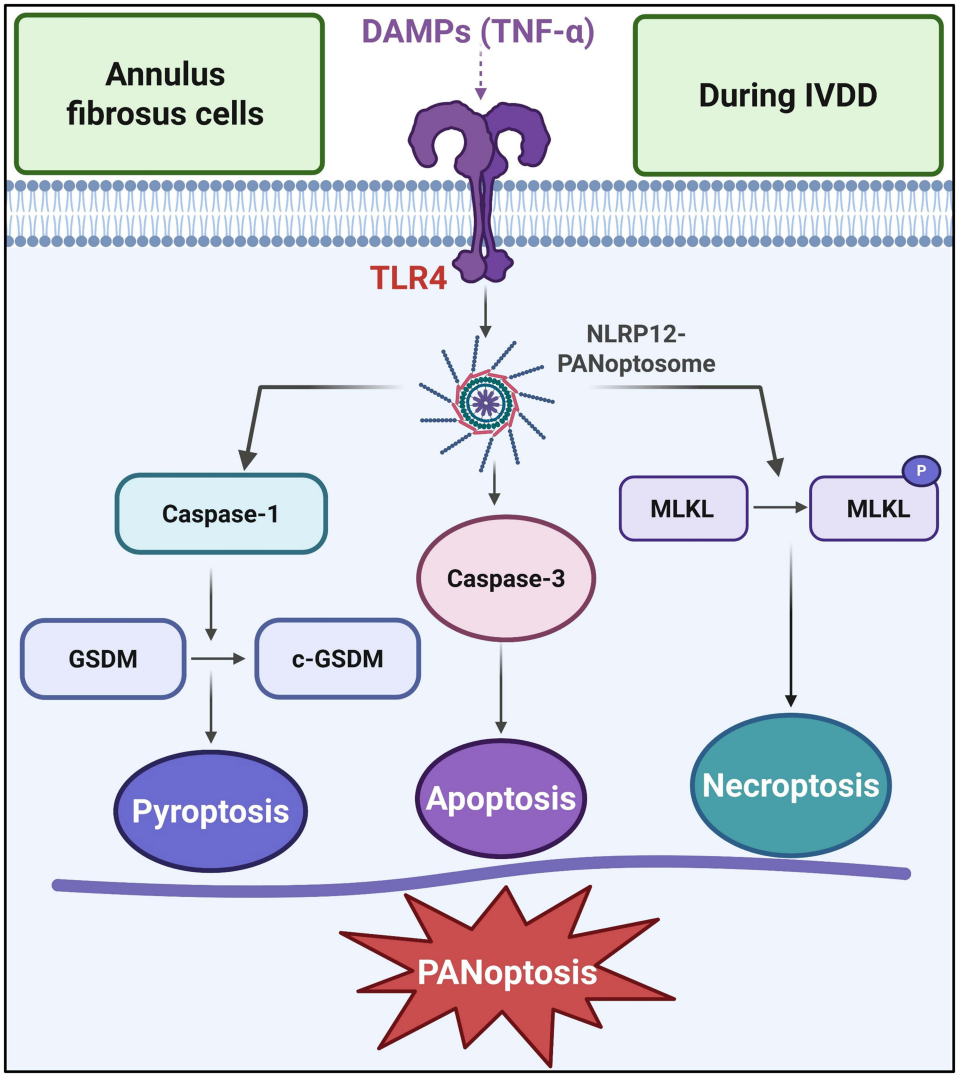

Figure 6 Schematic diagram of TLR4 induces annulus fibrosus cells PANoptosis via NLRP12 in IVDD.

and clinical tissue samples were not included, which limits the translational relevance of the conclusions. Additionally, while our data support the involvement of the TLR4-NLRP12 axis in PANoptosis, the complexity of disc degeneration may involve additional regulatory pathways not addressed in this study. In future studies, we will aim to validate these findings in human IVD tissues and further explore their therapeutic potential.

Conclusion

Our study is the first to identify the occurrence of PANoptosis and PANoptosome formation in AFCs. We demonstrated that TLR4 promotes PANoptosis in AFCs through NLRP12 activation, contributing to IVDD progression, while TLR4 knockdown alleviates disc degeneration. These findings suggest that TLR4 may serve as a potential therapeutic target for IVDD.

Data Sharing Statement

All data and materials are included in this manuscript.

Ethics Approval

The animal study protocol was approved by the Ethics Committee of Qinghai Provincial People's Hospital (protocol code: KYLs (2024)-073, January 2024). All procedures were performed in accordance with the 3R principles (Replacement, Reduction, Refinement) to minimize animal suffering. For the scRNA-seq data analysis, since we utilized a publicly available dataset where all personally identifiable information had been anonymized by the data provider, this study was granted an exemption from ethical approval by the Ethics Committee of Qinghai Provincial People's Hospital.

Author Contributions

All authors made a significant contribution to the work reported, whether that is in the conception, study design, execution, acquisition of data, analysis and interpretation, or in all these areas; took part in drafting, revising or critically reviewing the article; gave final approval of the version to be published; have agreed on the journal to which the article has been submitted; and agree to be accountable for all aspects of the work.

Funding

This work was supported by 2022 Kunlun Talents of Qinghai Province High-end Innovation and Entrepreneurship - Cultivate Leading Talents Project [QHKLYC-GDCXCY-2022-058] and the Health Committee Key Project in Qinghai Province [2022-wjzd-02].

Disclosure

The authors report no conflicts of interest in this work.

References

1. Kuzu Ş, Canli M, Valamur İ, Özüdoğru A, Alkan H, Hartavi A. Effects of aerobic exercise in addition to core stabilization exercises on functional capacity, physical performance and fall risk in geriatric individuals with chronic non-specific low back pain. *BMC Sports Sci Med Rehab*. 2025;17(1):211–218. doi:10.1186/s13102-025-01271-7
2. Zhu D, Liang H, Du Z, et al. Altered metabolism and inflammation driven by post-translational modifications in intervertebral disc degeneration. *Research*. 2024;7:350. doi:10.34133/research.0350
3. Moon HJ, Yurube T, Lozito TP, et al. Effects of secreted factors in culture medium of annulus fibrosus cells on microvascular endothelial cells: elucidating the possible pathomechanisms of matrix degradation and nerve in-growth in disc degeneration. *Osteoarthr Cartilage*. 2014;22(2):344–354. doi:10.1016/j.joca.2013.12.008
4. Zhang W, Wang H, Yuan Z, et al. Moderate mechanical stimulation rescues degenerative annulus fibrosus by suppressing caveolin-1 mediated pro-inflammatory signaling pathway. *Int J Biol Sci*. 2021;17(5):1395–1412. doi:10.7150/ijbs.57774
5. Sundaram B, Pandian N, Mall R, et al. NLRP12-PANoptosome activates PANoptosis and pathology in response to heme and PAMPs. *Cell*. 2023;186(13):2783–2801. doi:10.1016/j.cell.2023.05.005
6. Chen Y, Hu B, Ni F, et al. Kongensin a attenuates intervertebral disc degeneration by inhibiting TAK1-mediated PANoptosis of nucleus pulposus cells. *Int Immunopharmacol*. 2024;129:111661. doi:10.1016/j.intimp.2024.111661
7. Jacobsen TD, Yiantsos SO, Gansau J, Meyers J, Laudier D, Iatridis JC. TNFα receptor 1 and not receptor 2 affect annulus fibrosus and nucleus pulposus response to cytokine challenge in a rat model. *Jor Spine*. 2025;8(2):e70070. doi:10.1002/jsp2.70070

8. Liu C, Gao X, Lou J, et al. Aberrant mechanical loading induces annulus fibrosus cells apoptosis in intervertebral disc degeneration via mechanosensitive ion channel Piezo1. *Arthritis Res Ther*. 2023;25(1):117. doi:10.1186/s13075-023-03093-9
9. Yao S, Li Y, Ruan H, Wu L, Zeng H. Gubi decoction ameliorates porous cartilage endplate in an intervertebral disc degeneration model mouse through inhibition of NF-κB activity and pyroptosis. *J Inflammation Res*. 2025;18:5293–5309. doi:10.2147/JIR.S492365
10. Coutinho-Wolino KS, Almeida PP, Mafra D, Stockler-Pinto MB. Bioactive compounds modulating Toll-like 4 receptor (TLR4)-mediated inflammation: pathways involved and future perspectives. *Nutr Res*. 2022;107:96–116. doi:10.1016/j.nutres.2022.09.001
11. Huang L, Tao Y, Wu X, Wu J, Shen M, Zheng Z. The role of NLRP12 in inflammatory diseases. *Eur J Pharmacol*. 2023;956:175995. doi:10.1016/j.ejphar.2023.175995
12. Sun H, Wen X, Li H, et al. Single-cell RNA-seq analysis identifies meniscus progenitors and reveals the progression of meniscus degeneration. *Ann Rheum Dis*. 2020;79(3):408–417. doi:10.1136/annrheumdis-2019-215926
13. Tu J, Li W, Yang S, et al. Single-cell transcriptome profiling reveals multicellular ecosystem of nucleus pulposus during degeneration progression. *Adv Sci*. 2022;9(3):2103631. doi:10.1002/advs.202103631
14. Ji Q, Zheng Y, Zhang G, et al. Single-cell RNA-seq analysis reveals the progression of human osteoarthritis. *Ann Rheum Dis*. 2019;78(1):100–110. doi:10.1136/annrheumdis-2017-212863
15. Zollinger AJ, Smith ML. Fibronectin, the extracellular glue. *Matrix Biol*. 2017;60–61:27–37. doi:10.1016/j.matbio.2016.07.011
16. Swahn H, Mertens J, Olmer M, et al. Shared and compartment–specific processes in nucleus pulposus and annulus fibrosus during intervertebral disc degeneration. *Adv Sci*. 2024;11(17):e2309032. doi:10.1002/advs.202309032
17. Xie S, Li J, Lyu F, et al. Novel tripeptide RKH derived from Akkermansia muciniphila protects against lethal sepsis. *Gut*. 2024;73(1):78–91. doi:10.1136/gutjnl-2023-329996
18. Pandeya A, Kanneganti T. Therapeutic potential of PANoptosis: innate sensors, inflammasomes, and RIPKs in PANoptosomes. *Trends Mol Med*. 2024;30(1):74–88. doi:10.1016/j.molmed.2023.10.001
19. Yang W, Xu Y, Liu S, et al. Mebendazole induces ZBP-1 mediated PANoptosis of acute myeloid leukemia cells by targeting TUBA1A and exerts antileukemia effect. *J Adv Res*. 2025.
20. Bai M, Lei J, Li F, et al. Short-chain chlorinated paraffins may induce ovarian damage in mice via AIM2- and NLRP12-PANoptosome. *Environ Sci Technol*. 2025;59(1):163–176. doi:10.1021/acs.est.4c08622
21. Zhou T, Chen Y, Liao Z, et al. Spatiotemporal characterization of human early intervertebral disc formation at single-cell resolution. *Adv Sci*. 2023;10(14):e2206296. doi:10.1002/advs.202206296
22. Gao B, Jiang B, Xing W, Xie Z, Luo Z, Zou W. Discovery and application of postnatal nucleus pulposus progenitors essential for intervertebral disc homeostasis and degeneration. *Adv Sci*. 2022;9(13):e2104888. doi:10.1002/advs.202104888
23. Sundaram B, Pandian N, Kim HJ, et al. NLRC5 senses NAD+ depletion, forming a PANoptosome and driving PANoptosis and inflammation. *Cell*. 2024;187(15):4061–4077. doi:10.1016/j.cell.2024.05.034
24. Xiang Q, Geng Z, Yi X, Wei X, Zhu X, Jiang D. PANoptosis: a novel target for cardiovascular diseases. *Trends Pharmacol Sci*. 2024;45(8):739–756. doi:10.1016/j.tips.2024.06.002
25. Oh S, Lee J, Oh J, et al. Integrated NLRP3, AIM2, NLRC4, Pyrin inflammasome activation and assembly drive PANoptosis. *Cell Mol Immunol*. 2023;20(12):1513–1526. doi:10.1038/s41423-023-01107-9
26. Hou G, Chen Y, Lei H, et al. Bimetallic peroxide nanoparticles induce PANoptosis by disrupting ion homeostasis for enhanced immunotherapy. *Sci Adv*. 2024;10(45):eadp7160. doi:10.1126/sciadv.adp7160
27. Cheng Z, Gan W, Xiang Q, et al. Impaired degradation of PLCG1 by chaperone-mediated autophagy promotes cellular senescence and intervertebral disc degeneration. *Autophagy*. 2025;21(2):352–373. doi:10.1080/15548627.2024.2395797
28. Yu X, Zhao Y, Abudouaini H, et al. A novel spherical GelMA-HAMA hydrogel encapsulating APETx2 polypeptide and CFIm25-targeting sgRNA for immune microenvironment modulation and nucleus pulposus regeneration in intervertebral discs. *J Nanobiotechnol*. 2024;22(1):556. doi:10.1186/s12951-024-02783-z
29. Qin T, Shi M, Zhang C, et al. The muscle–intervertebral disc interaction mediated by L-BAIBA modulates extracellular matrix homeostasis and PANoptosis in nucleus pulposus cells. *Exp Mol Med*. 2024;56(11):2503–2518. doi:10.1038/s12276-024-01345-5
30. Henkel FDR, ONeill LAJ. NLRP12 drives PANoptosis in response to heme. *Trends Immunol*. 2023;44(8):574–576. doi:10.1016/j.it.2023.06.008
31. Sampara P, Banala RR, Vemuri SK, Av GR, Gpv S. Understanding the molecular biology of intervertebral disc degeneration and potential gene therapy strategies for regeneration: a review. *Gene Ther*. 2018;25(2):67–82. doi:10.1038/s41434-018-0004-0
32. Moldovan F. Correlation between peripheric blood markers and surgical invasiveness during humeral shaft fracture osteosynthesis in young and middle-aged patients. *Diagnostics*. 2024;14(11):1112. doi:10.3390/diagnostics14111112